

工學碩士 學位論文

# 64 QAM

A Study on the Effect of Phase Noise on 64 QAM System  
Performance

指導教授 趙 炯 來

2001年 2月

韓國海洋大學校 大學院

電波工學科 崔 正 洙

本 論 文   崔 正 洙   工 學 碩 士   學 位 論 文   認 准   .

委 員 長   :   工 學 博 士   金 東 一   ( 印 )

委 員   :   工 學 博 士   閔 庚 植   ( 印 )

委 員   :   工 學 博 士   趙 炯 來   ( 印 )

2001年 2月

韓 國 海 洋 大 學 校   大 學 院

電 波 工 學 科   崔 正 洙

Abstract .....	
Nomenclature .....	
1 .....	1
2 .....	3
2-1 .....	3
2-2 .....	5
2-3 PLL .....	7
2-4 .....	8
3 5 CMOS .....	11
3-1 .....	11
3-2 ISF .....	15
3-3 .....	21
4 .....	24
4-1 QPSK .....	24
4-1-1 .....	27
4-1-2 HP-ADS .....	29
4-2 64 QAM .....	36
5 .....	40
.....	41

## Abstract

In modern digital communication, Frequency synthesizers are widely used in wireless LAN, military radar and transceivers. In the military frequency hopping system, the 16 Kbps data are modulated to 14.5 MHz, up-converted to 30 88 MHz by frequency synthesizer, and transmitted through the channel. The received data are down-converted to IF band by frequency synthesizer and demodulated. Because transceivers rely heavily on frequency conversion using frequency synthesizer in hopping systems and ,therefore, the spectral purity of the internal oscillators in both the receiver and the transmitter is one of the factors limiting the maximum number of available channels and users. Also, these are demanded for wide-band frequency scope and excellent frequency resolution. To satisfy this conditions, we must predict the oscillator's internal phase noise and carefully consider when it designed.

The phase noise model proposed in [1] is widely known as the Leeson model, and is by far the most well-known. It is based on a linear time-invariant (LTI) approach for tuned tank oscillator, but it really has the nonlinear time variant natures. LC-tuned oscillator is using band-pass characteristics to reduce phase noise and has good performance than ring oscillator which has switching effect in power supply. However, it has not been used widely, for not be integrated on synthesizer.

Thus, in this thesis, linear time-variant(LTV) CMOS inverter ring oscillator's model which can be integrated and has good performance in phase noise than relaxation oscillator is analyzed.

To predict the phase noise of oscillator very accurately, the oscillator is considered, which has the linearly time-varying

nature when the input impulsive current into the oscillator is small. The performance which detect the corrupted signal by oscillator phase noise is compared with only affected by AWGN and analyze how much it degrade system performance for 64 QAM.

In accordance with phase noise level, QPSK system performance, using HP-ADS(Advanced Design System), has been analyzed and compared with the results which only affected by AWGN. Added -85 dBc phase noise at 10 kHz offset frequency into the system degraded the BER about 2 dB in QPSK and 4 dB in 64 QAM.

## Nomenclature

- $A$  : asymmetry of the waveform
- $C_n$  : Fourier coefficient
- $f'_{rise}$  : maximum slope during rising time
- $f'_{fall}$  : maximum slope during falling time
- $h(t)$  : impulse response
- $N$  : CMOS inverter stage number
- $P(\theta)$  : phase noise
- $P_s$  : total error probability
- $S_\phi(\ )$  : power spectrum of  $\phi(t)$
- $(x)$  : impulse sensitivity function
- $\Delta t_{VCO}$  : timing error
- $\sigma_{\Delta\phi}$  : phase jitter
- $\sigma_\tau$  : timing jitter
- $\phi(t)$  : excess phase

1

가 , 21 가 가 가  
가 .

(SFH)

, LAN

16

Kbps

14.5 MHz

30 88 MHz

14.5 MHz

PLL

가

FSK

(FH)

(LTI)

[1],[2].

가

가

. LC-tuned

(switching effect) 가 power supply  
LC-tuned 가 (Jitter)

가 가 relaxation  
(LTV)

2

PLL

3 5 CMOS

ISF(Impulse Sensitivity Function)

, CMOS

4

ADS(Advanced Design System)

QPSK

CMOS

64 QAM

5



2

2.1

가

(propagation delay)

가

A/D

가

RF

QPSK FSK  
PLL PLL

PLL

PLL

, PLL

, power supply

AC

,  
가  
가

I/O

BER,

A/D

PLL

PLL

PLL

PLL

PLL VCO

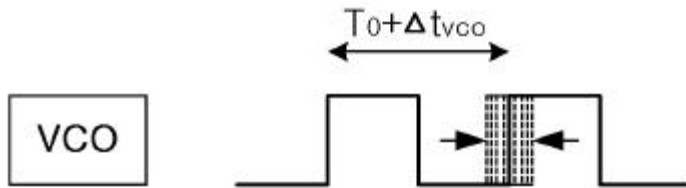
lock

(skew)

2.2

r.m.s (variation) .  $T_0$  가

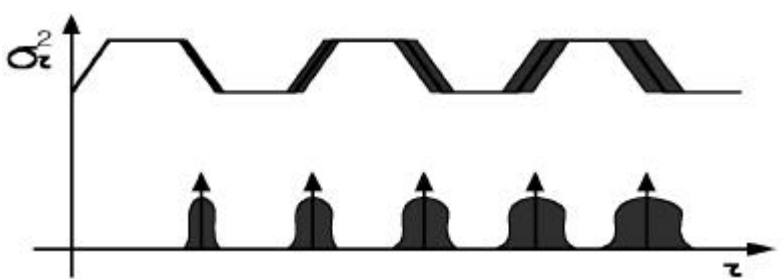
$\Delta t_{VCO}$  가 . 0  
 $\frac{\Delta t_{VCO}^2}{\Delta t_{VCO}^2}$  가 .



2-1. Cycle-to-Cycle

Fig. 2-1. Cycle-to-Cycle timing jitter

, ( z가 가  
 ) 가 .



2-2.

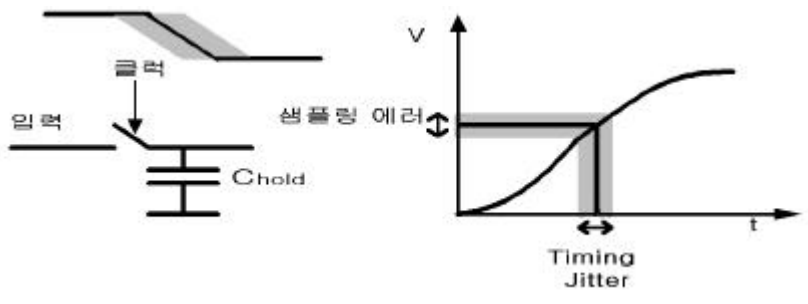
Fig. 2-2. Variance of timing jitter

가  $\tau$  r.m.s 가  $\sigma_\tau$  가 가

[3].

$$\sigma_{\Delta\phi} = 2\pi \frac{\sigma_\tau}{T} = \sigma_\tau \quad (2.1)$$

, T



2-3.

Fig. 2-3. Timing jitter and sampling error

$V_0 \sin(\omega_0 t)$ 가 sample/hold

가  $\sigma_\tau$  가  $\sigma_v$

$$\sigma_v = v_0 \omega_0 \cos(\omega_0 t) \sigma_\tau \quad (2.2)$$

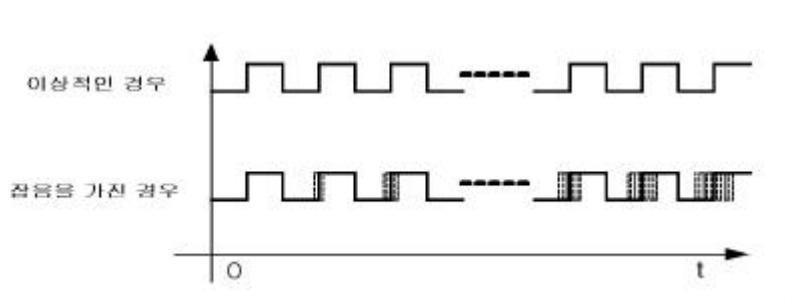
, 가 SNR (2.2) [3].

$$SNR = \frac{v_0^2/2}{\sigma_{v,ave}^2} = \frac{v_0^2/2}{v_0^2 \frac{\sigma_z^2/2}{v_0^2}} = \frac{1}{\sigma_z^2} \quad (2.3)$$

,  $\sigma_{v,ave}$  가

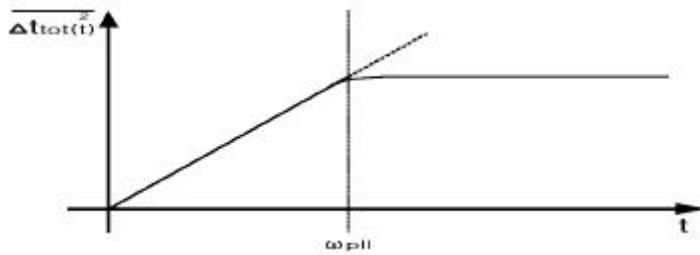
### 2.3 PLL

PLL VCO, PLL PLL PLL PLL PLL VCO PLL



2-4.

Fig. 2-4. Oscillator's timing jitter



2-5. PLL

Fig. 2-5. PLL output jitter

2-5 t가 VCO  
t가

, PLL

$$\overline{\Delta t_{PLL}^2} = \alpha^2 \cdot \overline{\Delta t_{VCO}^2} \quad (2.4)$$

,  $\alpha \approx \sqrt{\frac{f_{ref}}{2 f_{pll}}}$

2.4

[3].

$$\begin{aligned} \sigma_\tau^2 &= \frac{1}{2} E ( [\phi(t+\tau) - \phi(t)]^2 ) \\ &= \frac{E[\phi^2(t)]}{2} + \frac{E[\phi^2(t+\tau)]}{2} - \frac{E[\phi(t)\phi(t+\tau)]}{2} \end{aligned} \quad (2.5)$$

$$\begin{aligned} \sigma_x^2 &= E[(X - \bar{X})^2] = \int_{-\infty}^{\infty} (X - \bar{X})^2 f_X(X) dX \\ &= E[X^2 - 2X\bar{X} + \bar{X}^2] = E[X^2] - E^2[X] \end{aligned} \quad (2.6)$$

$\sigma_\tau$  가 가

$$\sigma_{\Delta\phi}(\Delta\phi) = 2\pi \frac{\sigma_\tau}{T} = \sigma_\tau \quad (2.7)$$

$$\sigma_{\tau} = \frac{1}{0} \sigma_{\Delta\phi} = \frac{1}{0} E [\phi(t+\tau) - \phi(t)] \quad (2.8)$$

$$\sigma_{\tau}^2 = \frac{1}{2} E [ [\phi(t+\tau) - \phi(t)]^2 ] \quad (2.9)$$

$$(2.9) \quad \phi(t) \quad R_{\phi}(\tau)$$

$$R_{\phi}(\tau) = E[\phi(t)\phi(t+\tau)] \quad (2.10)$$

(2.9)

$$\sigma_{\tau}^2 = \frac{2}{0} [R_{\phi}(0) - R_{\phi}(\tau)] \quad (2.11)$$

Khinchin theorem

$$R_{\phi}(\tau) = \frac{1}{2\pi} \int_{-\infty}^{\infty} S_{\phi}(\omega) e^{j\omega\tau} d\omega \quad (2.12)$$

$$S_{\phi}(\omega) = \frac{1}{T} \int_{-\infty}^{\infty} R_{\phi}(\tau) e^{-j\omega\tau} d\tau \quad (2.13)$$

$$S_{\phi}(\omega) = \phi(t) \quad (2.12)$$

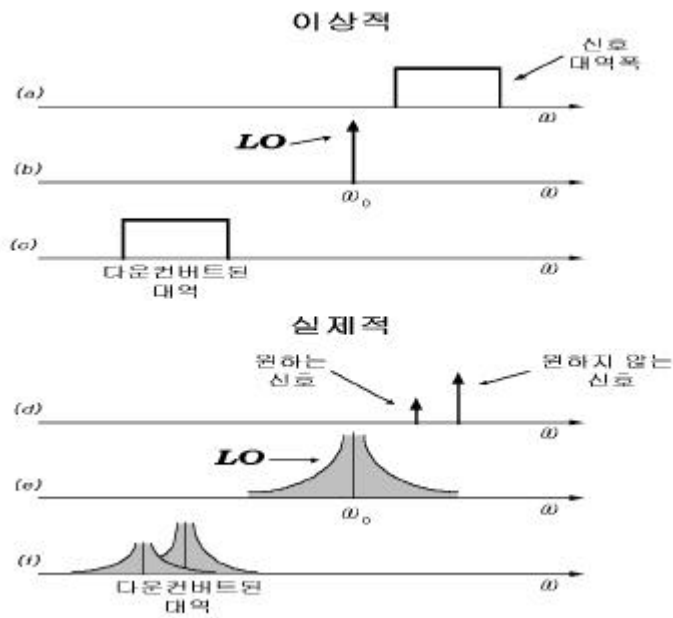
$$\sigma_{\tau}^2 = \frac{4}{\pi} \int_0^{\infty} S_{\phi}(\tau) \sin^2\left(\frac{\tau}{2}\right) d\tau \quad (2.14)$$



### 3 5 CMOS

#### 3.1

가 .  
 가 .  
 가 .



3-1.

Fig. 3-1. Effect of oscillator's phase noise on receiver

,  
 가

[4].

$$= \text{-----} \quad (3.1)$$

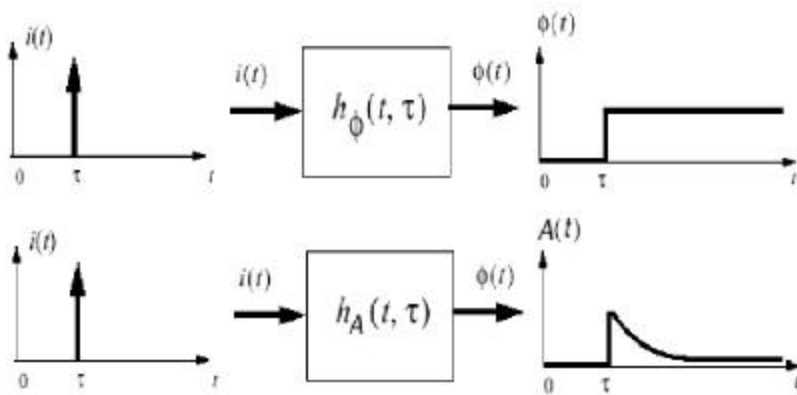
가

가  
(reciprocal mixing)

가

가

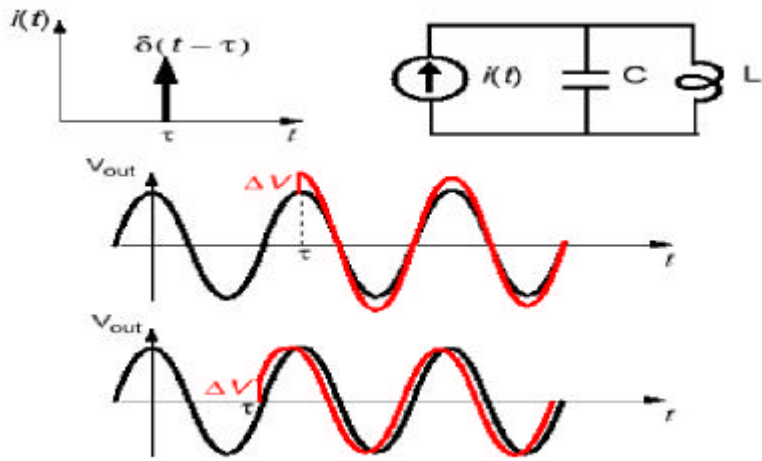
[3].



3-2.

가

Fig. 3-2. The equivalent system for oscillator's output phase and amplitude



### 3-3. LC

Fig. 3-3. Impulsive response of LC-tuned oscillator

LC

$V_0$

$$v(t) = V_0 \cos(\omega t)$$

(3.2)

$$i(t) = V_0 \sqrt{\frac{C}{L}} \sin(\omega t)$$

,  $v(t)$  ,  $i(t)$

,  $t = t_0$   $\Delta q$  가 가

$$\frac{\Delta q}{C} = \Delta V$$

,  $\Delta q$

,  $t_0^+$

$$v(t) \Big|_{t=t_0^+} = V_0 \cos(\omega t) + \frac{\Delta q}{C} \quad (3.3)$$

가  $t_0$  에서  $\Delta\phi$  가

$$\begin{aligned} v(t) &= (V_0 + \Delta V) \cos(\omega t + \Delta\phi) \\ i(t) &= (V_0 + \Delta V) \sqrt{\frac{C}{L}} \sin(\omega t + \Delta\phi) \end{aligned} \quad (3.4)$$

$$(3.4) \quad t_0^+$$

$$\begin{aligned} (V_0 + \Delta V) \cos(\omega t_0 + \Delta\phi) &= V_0 \cos(\omega t_0) + \frac{\Delta\phi}{C} \\ (V_0 + \Delta V) \sin(\omega t_0 + \Delta\phi) &= V_0 \sin(\omega t_0) \end{aligned} \quad (3.5)$$

$$(3.5)$$

$$\Delta\phi = - \frac{\Delta q}{C V_0} \sin(\omega t_0) \quad (3.6)$$

$$h_\phi(t, \tau) = \frac{- \sin(\omega \tau)}{q_{\max}} u(t - \tau) \quad (3.7)$$

가

3-3

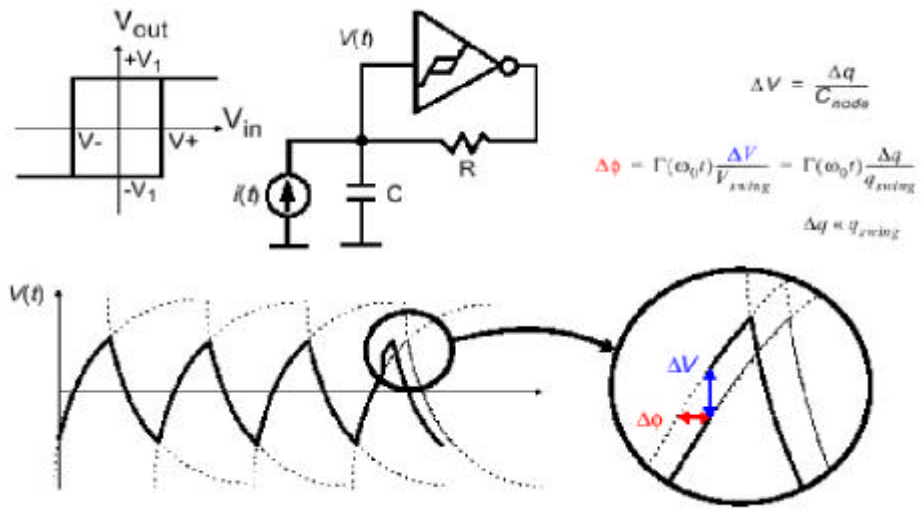
가 0

(excess phase)  $\phi(t)$

AGC

3-4 relaxation  
가

$$t = \tau$$



### 3-4. Relaxation

Fig. 3-4. Relaxation oscillator

## 3.2 ISF

3-4  $\Delta \phi$   
 $\Delta V$   
 ,  $\Delta \phi$

$$\Delta \phi = \left( \frac{\Delta V}{V_{max}} \right) = \left( \frac{\Delta q}{q_{max}} \right) \quad (3.8)$$

$$q_{max} = C_{node} V_{max}$$

, (x) ISF

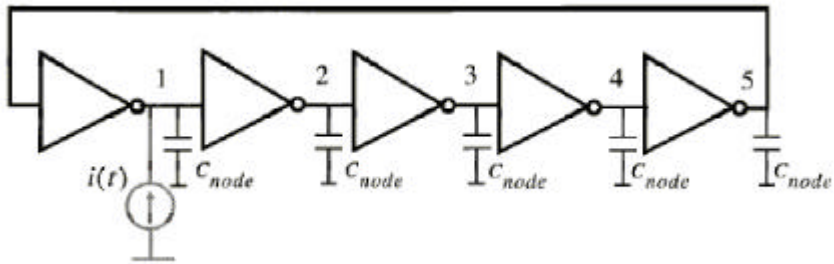
가

, 3-5

가 5 CMOS

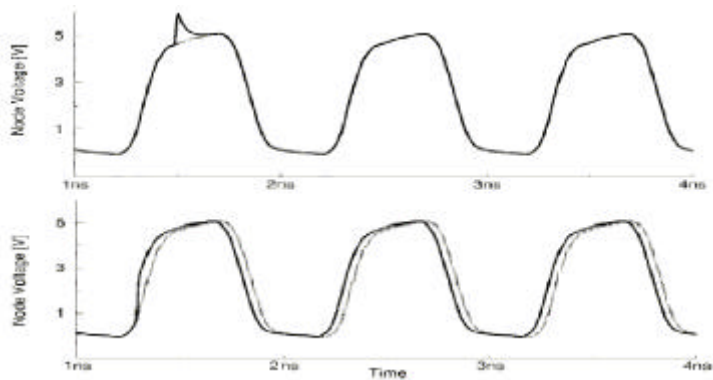
, 가  $t = \tau$   $\Delta q$  가

3-6



### 3-5. 5 CMOS

Fig. 3-5. 5-stage CMOS inverter ring oscillator



3-6.

Fig. 3-6. Phase shift

,

가

가

,

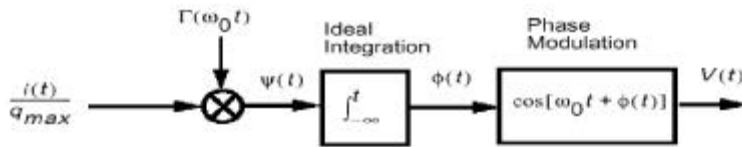
3-2

가 [3].

$$h_{\phi}(t, \tau) = \frac{(\quad \tau)}{q_{\max}} u(t - \tau) \quad (3.9)$$

,  $u(t)$

$$\begin{aligned} \phi(t) &= \int_{-\infty}^{\infty} h_{\phi}(t, \tau) i(\tau) d\tau \\ &= \int_{-\infty}^t \frac{(\quad \tau)}{q_{\max}} i(\tau) d\tau \end{aligned} \quad (3.10)$$



3-7. 가

Fig. 3-7. The equivalent block diagram of the process

ISF

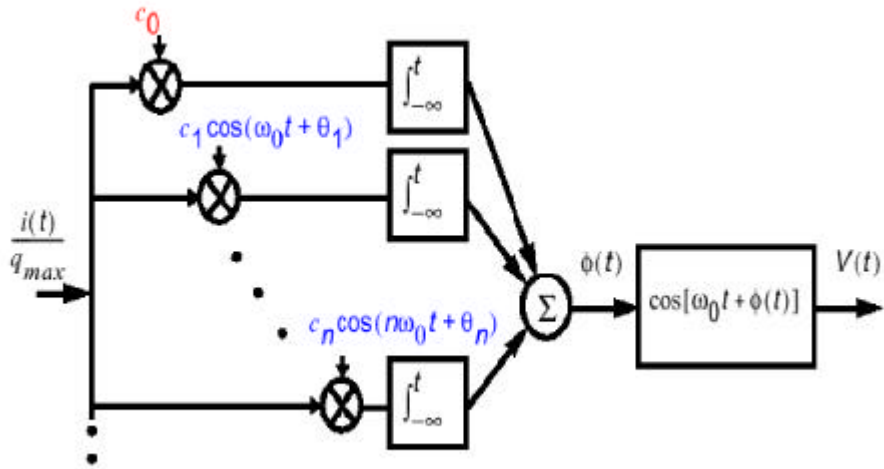
$$(\quad \tau) = c_0 + \sum_{n=1}^{\infty} c_n \cos(n \quad \tau + \theta_n) \quad (3.11)$$

,  $c_n$

$\theta_n$  n

(3-9), (3-10), (3-11)

$$\phi(t) = \frac{1}{q_{\max}} \left[ c_0 \int_{-\infty}^t i(\tau) d\tau + \sum_{n=1}^{\infty} c_n \int_{-\infty}^t i(\tau) \cos(n \omega_0 \tau) d\tau \right] \quad (3.12)$$



3-8. ISF 가

Fig. 3-8. The equivalent system for ISF

$$\phi(t) \approx \frac{I_n C_n \sin(\Delta t)}{2 q_{\max} \Delta} \quad (3.13)$$

(3.13)

$$\mathfrak{L}\{\Delta w\} = 10 \log \left( \frac{\frac{i_n^2}{\Delta f} \sum_{n=0}^{\infty} c_n^2}{4 q_{\max}^2 \Delta w^2} \right) \quad (3.14)$$

$$\frac{I_n^2}{2} = \frac{i_n^2}{\Delta f}, \quad (\Delta f = 1\text{Hz})$$



$$\frac{i_n^2}{\Delta f}$$

, Parseval

$$\sum_{n=0}^{\infty} c_n^2 = \frac{1}{\pi} \int_0^{2\pi} |f(x)|^2 dx = 2 i_{rms}^2 \quad (3.15)$$

$$\xi\{\Delta w\} = 10 \log \left( \frac{\frac{i_n^2}{\Delta f}}{2 q_{max}^2 \Delta w^2} \right) \quad (3.16)$$

ISF

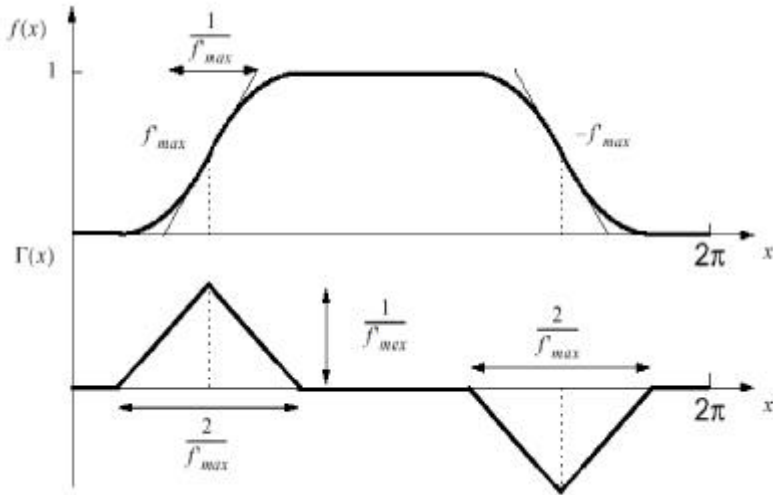
3-9

ISF

$$\frac{1}{f'_{max}}$$

가

,  $f'_{max} =$



3-9.

ISF

Fig. 3-9. Approximate waveform and ISF for a ring oscillator

• *rms* •

$$\begin{aligned}
 rms^2 &= \frac{1}{2\pi} \int_0^{2\pi} f^2(x) dx \\
 &= \frac{4}{2\pi} \int_0^{\frac{1}{f'_{max}}} x^2 dx \\
 &= \frac{2}{3\pi} \left( \frac{1}{f'_{max}} \right)^3
 \end{aligned}
 \tag{3.17}$$

1  
2N

*rms*

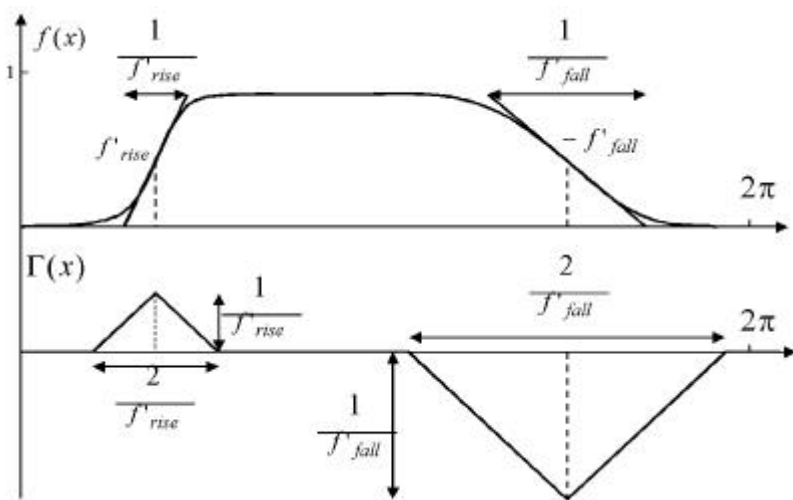
1

$$rms = \sqrt{\frac{2\pi^2}{3\eta^3}} \cdot \frac{1}{N^{1.5}}
 \tag{3.18}$$

3-10

ISF *r.m.s*

ISF



3-10.

ISF

Fig. 3-10. Approximate waveform and ISF for asymmetric rising and falling edges

$$\begin{aligned}
 f_{rms}^2 &= \frac{1}{\pi} \left[ \int_0^{\frac{1}{f'_{rise}}} x^2 dx + \int_0^{\frac{1}{f'_{fall}}} x^2 dx \right] \\
 &= \frac{1}{3\pi} \left( \frac{1}{f'_{max}} \right)^3 (1 + A^3)
 \end{aligned} \tag{3.19}$$

,  $f'_{rise}, f'_{fall} =$

$$A = \frac{f'_{rise}}{f'_{fall}}$$

,

$$2\pi = \eta N \left( \frac{1}{f'_{rise}} + \frac{1}{f'_{fall}} \right) = \frac{\eta N}{f'_{rise}} (1 + A) \tag{3.20}$$

, (3.19) (3.20) ,

$$f_{rms}^2 = \frac{8\pi^2}{3\eta^3} \cdot \frac{1}{N^3} \left[ \frac{1 + A^3}{(1 + A)^3} \right] \tag{3.21}$$

가

### 3.3

Leeson VHF lower UHF

[1].

$$l(f) [dB c/Hz] = 10 \log \left( 1 + \frac{f_o^2}{(2fQ)^2} * \left( 1 + \frac{f_c}{f} \right) \frac{NFKT}{2P_s} + \frac{2KTRK_o^2}{f^2} \right) \tag{3.22}$$

,  $f =$  ,  $NF =$  ,  $K_o =$  (Hz/ V),

$K =$  Boltzmann's constant =  $1.38 * 10^{-23}$  J/ K,  $T =$  =298K,

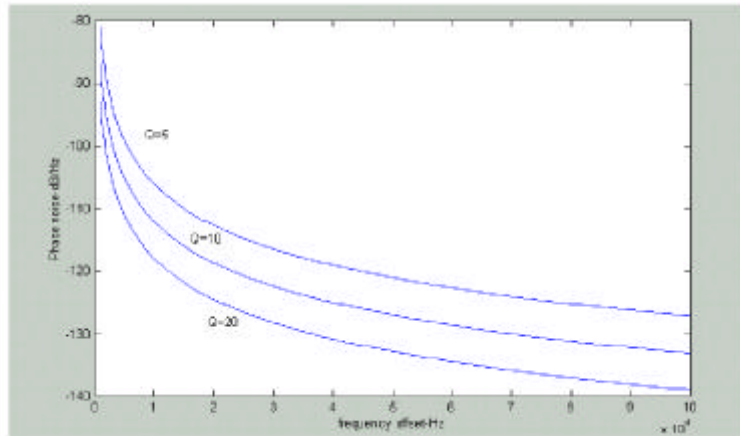
$R =$  가 ,  $P_s =$  ,

$f_c =$

,  $f_0 =$

, Leeson

Q

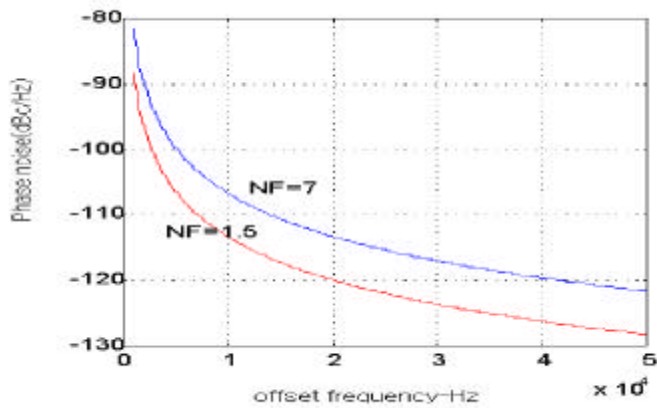


3-11. Q

Fig. 3-11. Phase noise for different values of oscillator Q

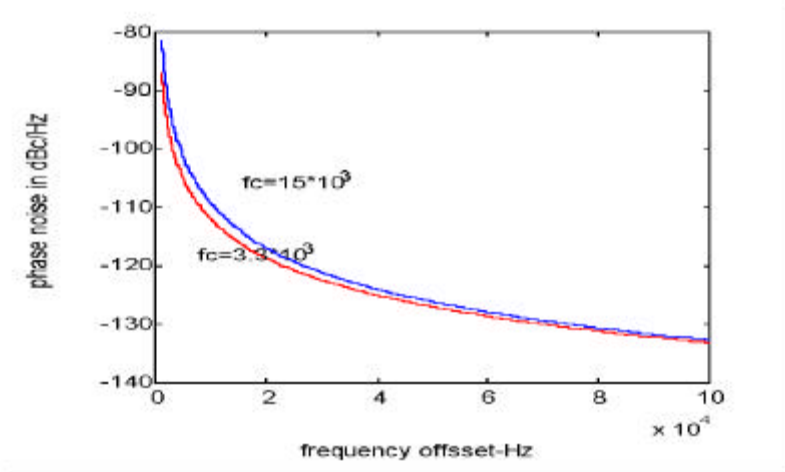
, FET가 BJT

FET BJT



3-12.

Fig. 3-12. Phase noise for different values of oscillator NF



3-13.

Fig. 3-13. Phase noise for different values of oscillator  $f_c$

10 30 dB

[5].

4

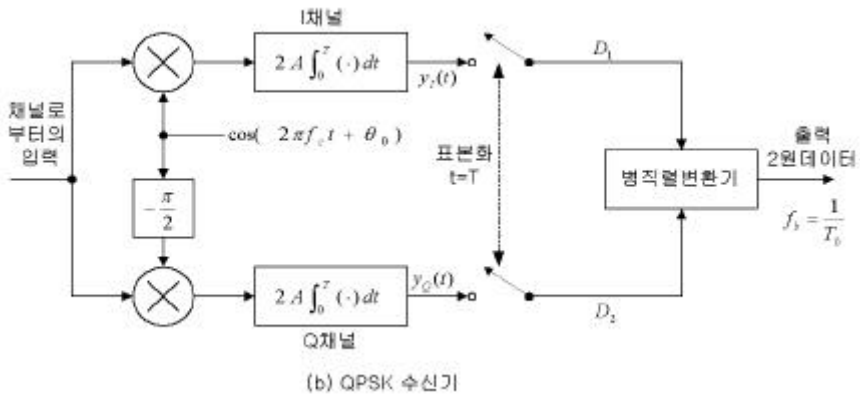
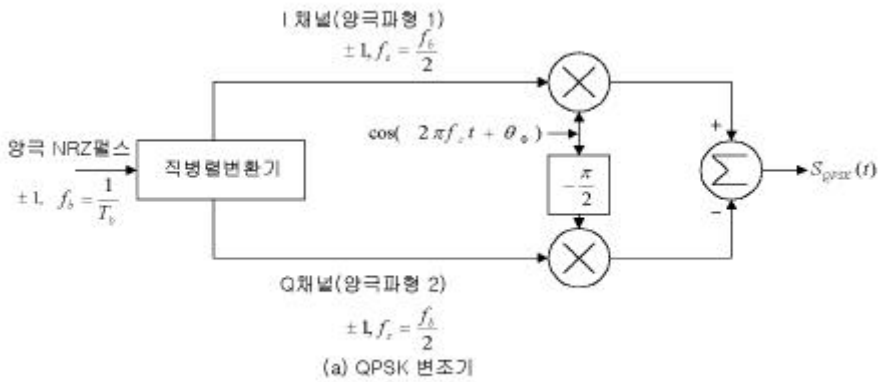
### 4.1 QPSK

PSK

$M = 2^m$  PSK,  $M = 2, 4, 8, \dots$  PSK

가 QPSK

가



4-1. QPSK

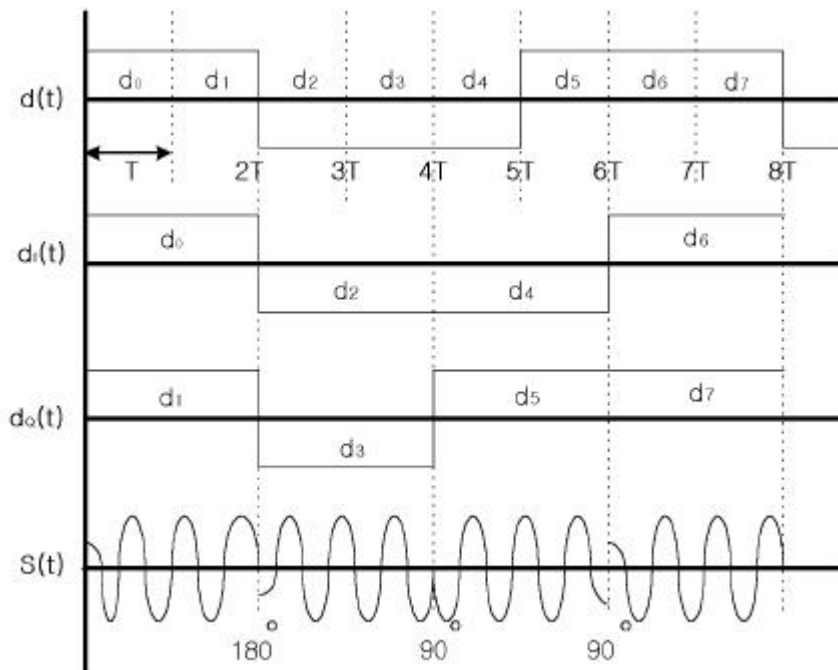
Fig. 4-1. QPSK modulator and receiver

(a) QPSK modulator (b) QPSK receiver

1.

Table 1. Signals and phases

$d_I(t)$	$d_Q(t)$	$S(t)$
1	1	$\cos \omega t - \sin \omega t = 2 \cos(\omega t + 45^\circ)$
-1	1	$-\cos \omega t - \sin \omega t = 2 \cos(\omega t + 135^\circ)$
1	-1	$\cos \omega t + \sin \omega t = 2 \cos(\omega t - 45^\circ)$
-1	-1	$-\cos \omega t + \sin \omega t = 2 \cos(\omega t + 225^\circ)$



4-2. QPSK

Fig. 4-2. QPSK modulated signals

, BPSK QPSK

, BPSK

$$P(e) = \frac{1}{2} \operatorname{erfc} \left( \sqrt{\frac{E_b}{N_0}} \right), \quad E_b = \frac{A^2 T}{2} \quad (4.1)$$

, QPSK

$$P(e) \simeq \operatorname{erfc} \sqrt{\frac{E_b}{N_0}}, \quad E_b = \frac{A^2 T_b}{2} \quad (4.2)$$

BPSK

$E_b/N_0$  SNR BPSK QPSK 3 dB

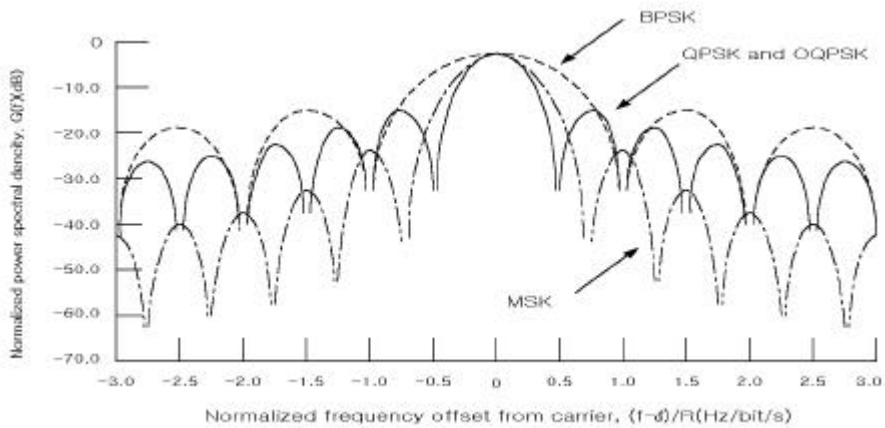
T QPSK BPSK 2

OQPSK QPSK 가 ,

/2 가

30%가 . , OQPSK

QPSK



#### 4-3. BPSK, QPSK, OQPSK MSK

Fig. 4-3. Normalized power spectrum density of BPSK, QPSK, OQPSK, and MSK



### 4.1.1

(correlation)  $\cos \theta$  , QPSK  
 cross coupling  $\sin \theta$   
 AWGN  
 QPSK [6].

$$p(\theta) = Q[(2 E_b / N_0)^{1/2} \rho(\theta)] \quad (4.3)$$

$$Q[v] \cong \frac{1}{(2\pi)^{1/2}} \int_v^{\infty} \exp(-\lambda^2/2) d\lambda \quad (4.4)$$

,  $\rho(\theta) = \theta$  (tracking) 가 ,  
 ,  $\rho = 1$   $\sqrt{2(E_b)}$  가  
 ,  $\theta$ 가  $\cos \theta$   
 가 [6].

가 QPSK  
 $\theta \neq 0$   $\cos \theta$   
 QPSK 2 . 2  
 $\pm \sin \theta$  ,  
 $\phi$  가 .

$$\rho_Q(\theta) = \cos \theta \pm \sin \theta \quad (4.5)$$

$$p_Q(\theta) = \frac{1}{2} [p_+(\theta) + p_-(\theta)] \quad (4.6)$$

$$p_+(\theta) = Q[(2 E_b / N_0)^{1/2}] (\cos \theta + \sin \theta)$$

$$p_-(\theta) = Q[(2 E_b / N_0)^{1/2}] (\cos \theta - \sin \theta)$$

[7],[8].

$$P(\theta) = \frac{1}{\sqrt{2\pi\sigma^2}} e^{-\frac{\theta^2}{2\sigma^2}} \quad (4.7)$$

$$\sigma^2 = \theta_{rms}^2 + \overline{\theta_{no}^2}$$

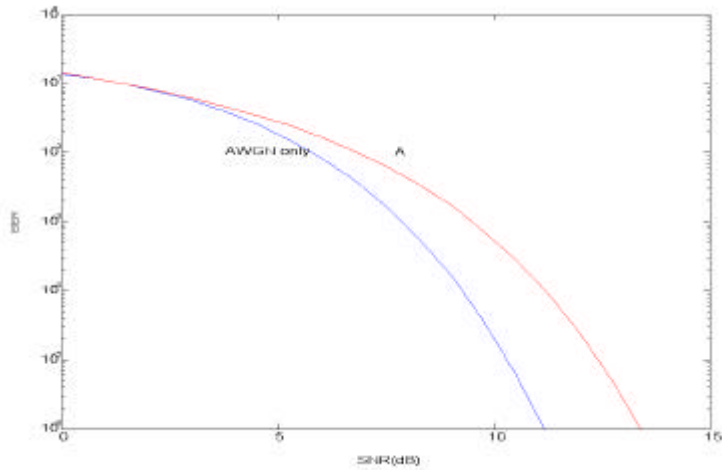
$$\frac{\theta_{rms}^2}{\overline{\theta_{no}^2}} \quad \text{AWGN} \quad \text{PLL}$$

, i

$\theta$

i

$$P_{si} = \int_{-\pi}^{\pi} P(\theta) p_Q(\theta) \quad (4.8)$$

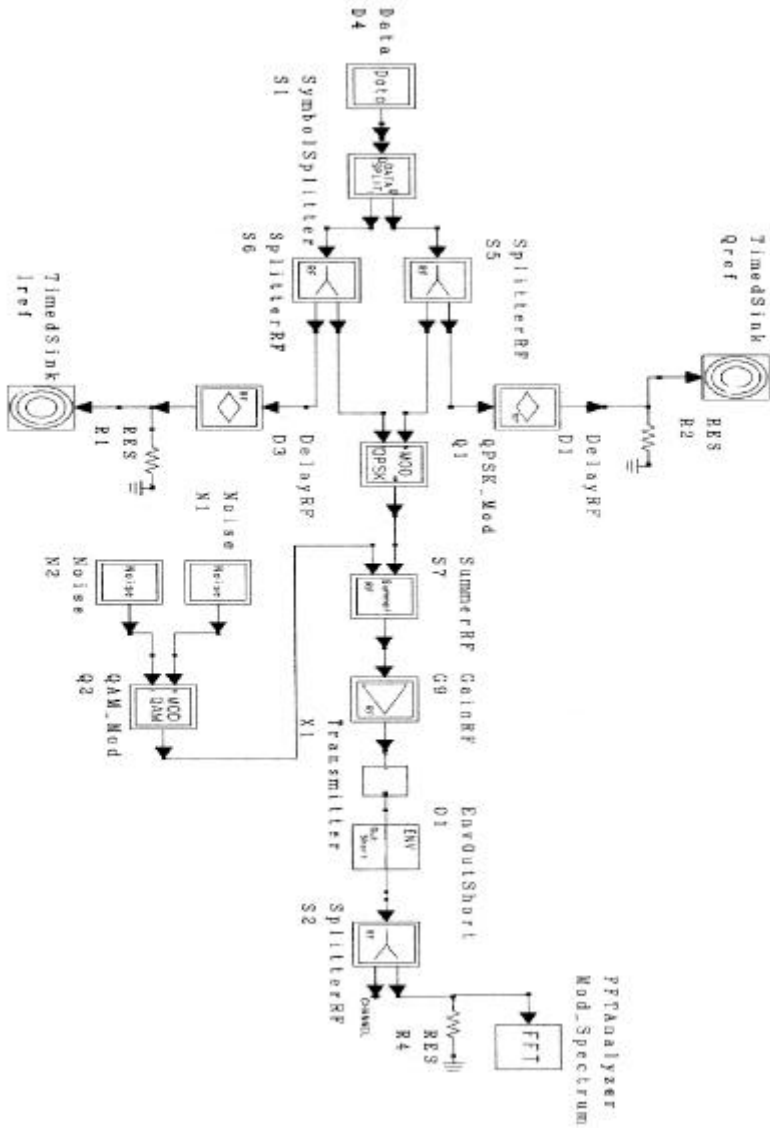


4-4. QPSK BER

Fig. 4-4. QPSK BER curves, affected by phase noise

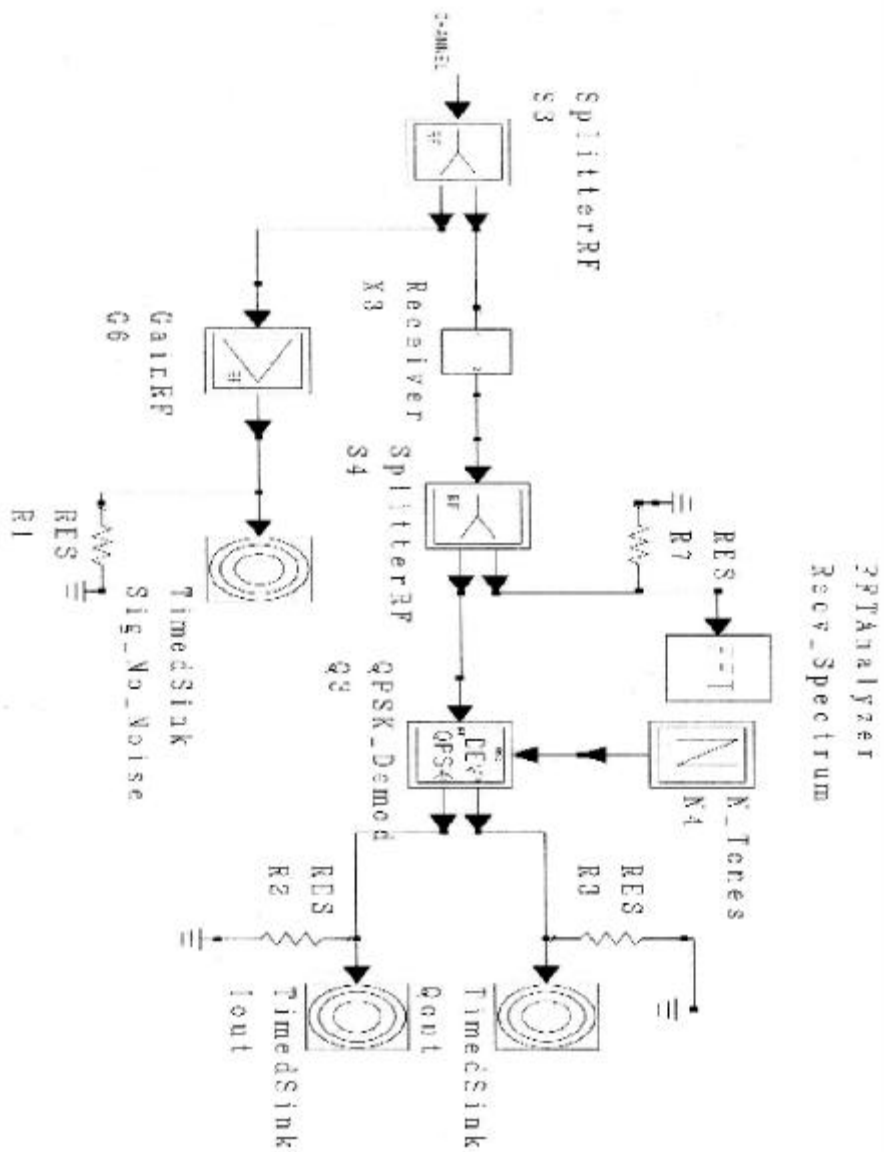
, A 4.12 10 kHz -85 dBc/ Hz

### 4.1.2 ADS



### 4-5. QPSK

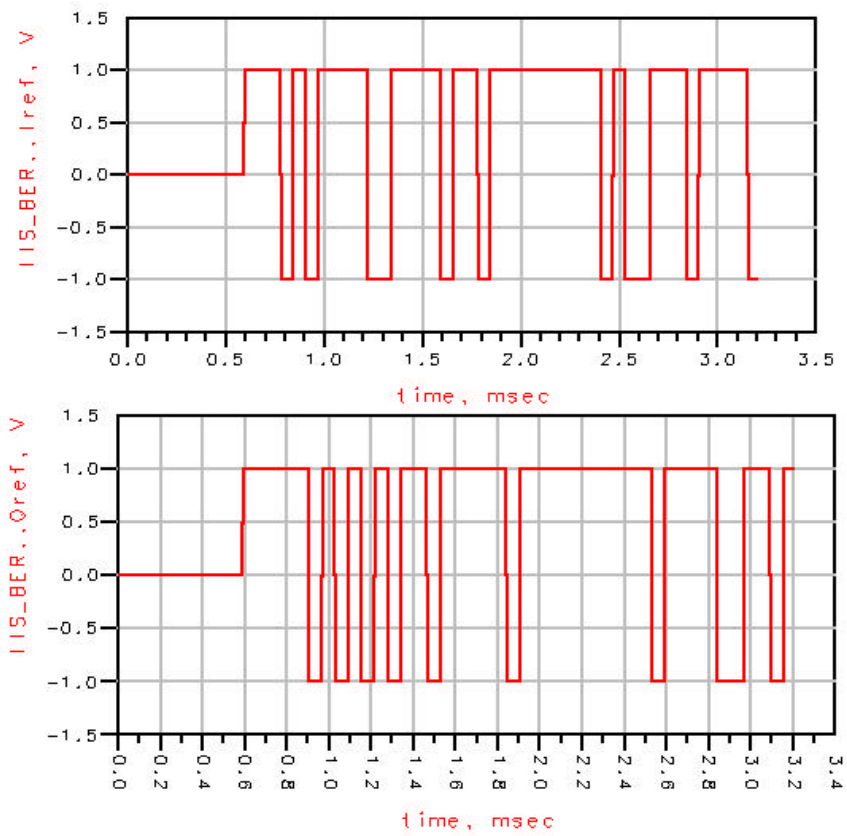
Fig. 4-5. QPSK transmitter



4-6. QPSK

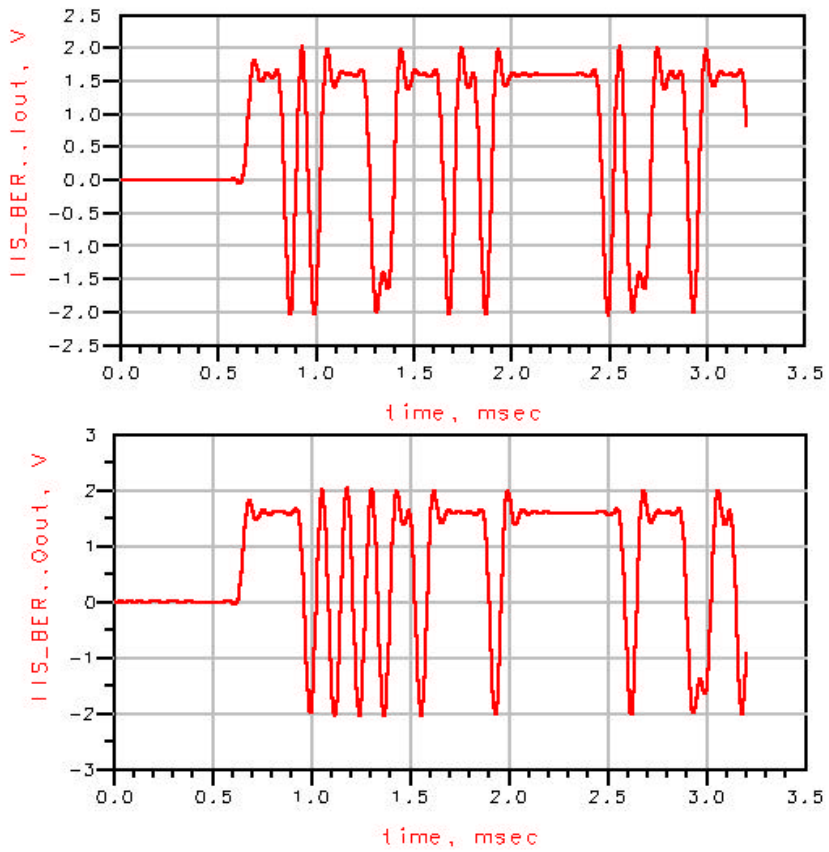
Fig. 4-6. QPSK receiver





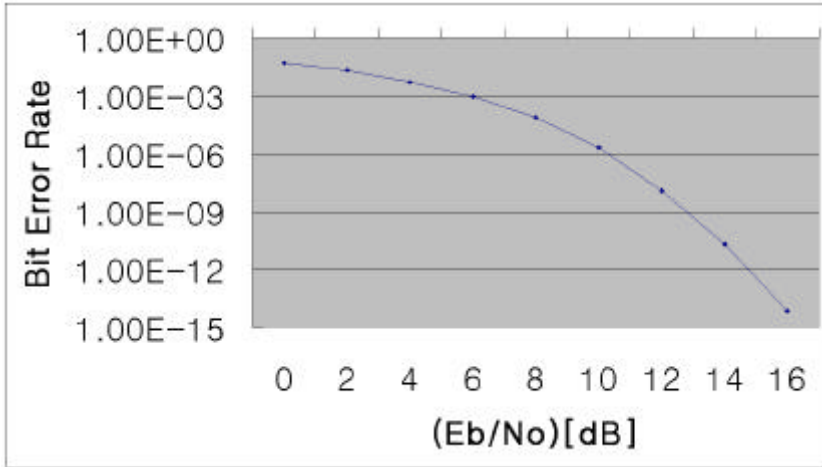
#### 4-8. QPSK I/Q

Fig. 4-8. QPSK I/Q channels input data



#### 4-9. QPSK I/Q

Fig. 4-9. QPSK I/Q channels output data

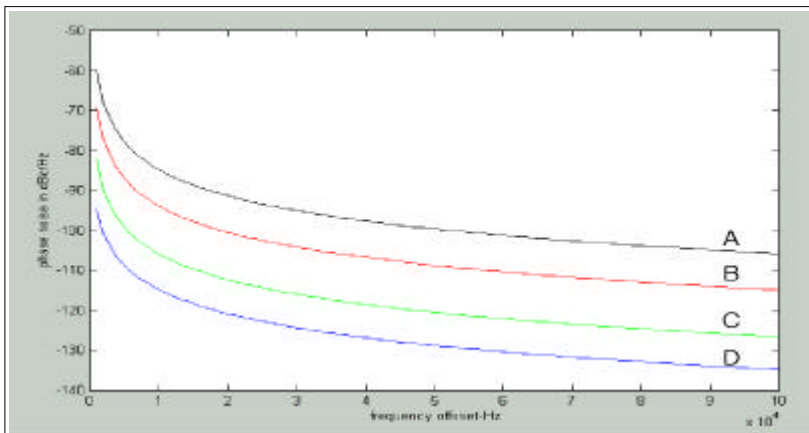


4-10. AWGN

QPSK BER

Fig. 4-10. QPSK BER curve, only affected by AWGN

4-10  
 10.5 dB  
 QPSK  
 ,  
 10<sup>-6</sup> E<sub>b</sub>/N<sub>0</sub> 가  
 ,  
 4-11 2



4-11.

Fig. 4-11. Phase noise levels



2. 10 kHz

Table 2. Phase noise levels at 10 kHz offset frequency

	A	B	C	D
10KHz offset (dBc/Hz)	-85	-95	-105	-115

ADS

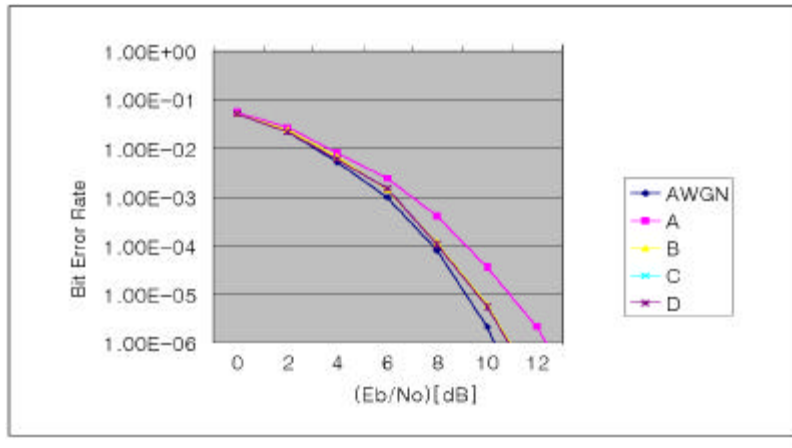
QPSK

3

3. BER

Table 3. BERs in accordance with phase noise levels

	A	B	C	D	only AWGN
$(10^{-6})$ $E_b / N_0$ (dB)	$\approx 12.4$	$\approx 10.10$	$\approx 10.9$	$\approx 10.8$	$\approx 10.2$



4-12. BER

Fig. 4-12. BER curves for different phase noise levels

3

4-11

10 KHz

-95 dBc/ Hz

10 KHz  
 -85 dBc/ Hz  
 AWGN 2.2 dB

4.2 64 QAM

(QAM)  
 가

AWGN

(translation)

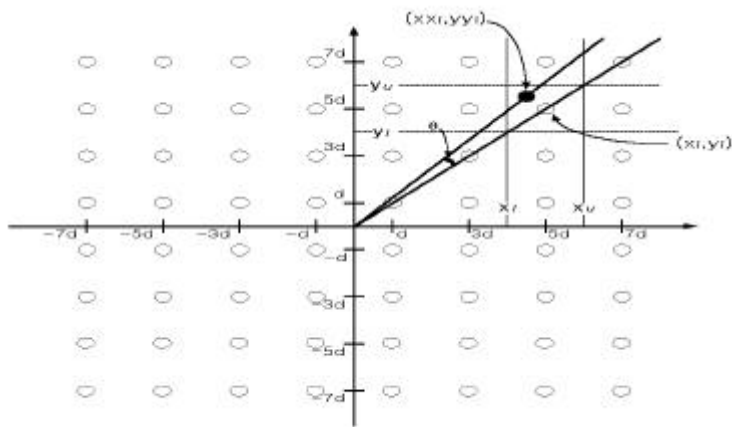
PLL

AWGN

가

(4.7)

(4.8)



4-13. i

Fig. 4-13. Probability of symbol error for i

4-13 i 가

$$P_{si}[\epsilon] = P_r[x_u < x_i + n_x < x_l] + P_r[y_u < y_i + n_y < y_l] \quad (4.9)$$

,  
 $x_u = x$  upper boundary  
 $x_l = x$  lower boundary  
 $y_u = y$  upper boundary  
 $y_l = y$  lower boundary  
 $n_x = x$   
 $n_y = y$

$$P_r[x_u < x_i + n_x < x_l] = P_r[n_x > x_u - x_i] + P_r[n_x > x_i - x_l] \quad (4.10)$$

$$P_r[n_x > x_u - x_i] = \int_{x_u - x_i}^{\infty} \frac{1}{\sqrt{2\pi\sigma^2}} e^{-\frac{l^2}{2\sigma^2}} dl \quad (4.11)$$

[9].

$(x_i, y_i)$

$(xx_i, yy_i)$

Cartesian

가

$$xx_i = \sqrt{x_i^2 + y_i^2} \left[ \cos \left[ \tan^{-1} \left( \frac{y_i}{x_i} \right) \right] \cos(\theta) - \sin \left[ \tan^{-1} \left( \frac{y_i}{x_i} \right) \right] \sin(\theta) \right] \quad (4.12)$$

$$yy_i = \sqrt{x_i^2 + y_i^2} \left[ \sin \left[ \tan^{-1} \left( \frac{y_i}{x_i} \right) \right] \cos(\theta) + \cos \left[ \tan^{-1} \left( \frac{y_i}{x_i} \right) \right] \sin(\theta) \right] \quad (4.13)$$

(4-12), (4-13)      (4-9)       $\theta$

(4-8)      i

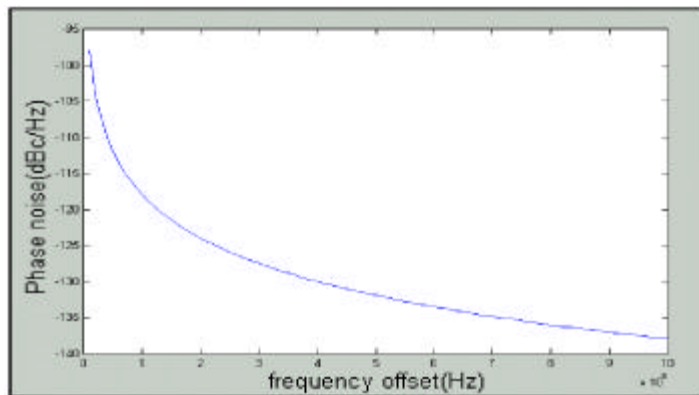
64

(equally

probable) 가

$$P_s = \frac{1}{M} \sum_{i=0}^{M-1} P_{si} \quad (4.14)$$

, M=64



4-14. 11

Fig. 4-14. Phase noise of 11-stage ring oscillator

4. 11

Table 4. Phase noise of 11-stage ring oscillator

offset frequency (kHz)	0.6	1	10	100	1000	10000
SSB noise density (dBc/ Hz)	-54	-58	-78	-98	-118	-138

16 kbps

가

HPF

tracked- out

가 1

2

2%

[10].

64 kbps

1.2 kHz

600 Hz

600 Hz

600 Hz 10

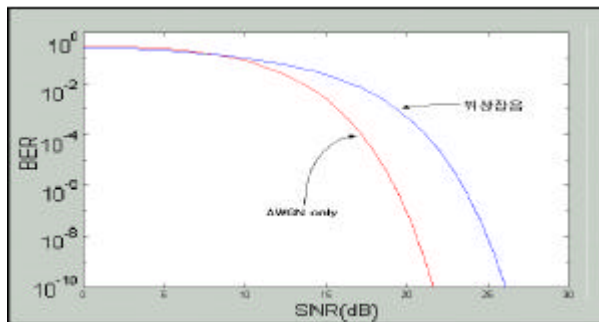
MHz

r.m.s

0.082 rad

degree

가 4.69 °



4-15.

BER

Fig. 4-15. BER curves, affected by phase noise

5

가

. , QPSK HP-ADS HP-ADS 가  
 HP-ADS 64 QAM  
 , PLL  
 QPSK 가 ADS QPSK  
 QPSK .  
 , AWGN  
 . 10 kHz  
 -85 dBc, -95 dBc, -105 dBc, -115 dBc  
 가 BER -105 dBc 가 BER  
 AWGN  
 QPSK 64 QAM AWGN  
 QPSK 10 kHz  
 -85 dBc/ Hz AWGN  
 64 QAM  $E_b/N_0$  가 2 dB  $E_b/N_0$ 가  
 4 dB  
 ,  
 ,  
 가 .

- [1] D. B. Leeson, "A simple model of feedback oscillator noise spectrum," *Proc. IEEE*, vol. 54, pp. 329-330, Feb. 1966
- [2] B. Razavi, "A study of phase noise in CMOS oscillators," *IEEE J. Solid-State Circuits*, vol. 31, pp. 331-343, Mar. 1996.
- [3] A. Hajimiri, T. H. Lee and T. H. Lee, *The design of Low Noise Oscillators*, KAP, 1999.
- [4] J. Craninx and Michiel Steyaert, "Low-Noise Voltage-Controlled Oscillators Using Enhanced LC-Tanks," *IEEE Transactions on Circuits and Systems- : Analog and Digital Signal Processing*, vol. 42, No. 12, pp. 794-804, Dec. 1995.
- [5] M. K. Nezami, "Evaluate The Impact Of Phase Noise On Receiver Performance," *Microwaves & RF*, pp. 165-172, May 1998.
- [6] S. A. Rhodes, "Effect of Noisy Phase Reference on Coherent Detection of Offset-QPSK Signals," *IEEE Transactions on Communications*," vol. COM-22, No. 8, pp. 1046-1055, Aug. 1974.
- [7] A. Papoulis, *Probability, Random Variables, and Stochastic Processes*, New York, McGraw-Hill , 1984.
- [8] F. Gardner, *Phaselock Techniques*, New York, John Wiley & Sons, 1979.
- [9] J. G. Proakis , *Digital Communications - Third edition*, New York, McGraw-Hill, 1995.
- [10] M. Kolber, "Predict Phase-Noise Effects In Digital Communication Systems," *Microwaves & RF*, pp. 59-70, May 1998.

가  
92  
가